Available online at www.sciencedirect.com
SCIENCE DIRECT
Journal of Molecular Graphics and Modelling 24 (2005) 128–137
Journal of Molecular Graphics and Modelling
www.elsevier.com/locate/JMGM

# Development of parameter sets for semi-empirical MO calculations of transition metal systems: Iron parameters for iron–sulfur proteins

Jonathan P. McNamara *, Mahesh Sundararajan, Ian H. Hillier

*School of Chemistry, University of Manchester, Manchester M13 9PL, UK*

Available online 24 August 2005

**Abstract**

A semi-empirical parameter set for iron has been developed which is appropriate for the study of iron–sulfur proteins having a single iron atom, by fitting to density-functional theory (DFT) calculations obtained for a series of small models of iron-containing proteins. These parameters are obtained using a modified BFGS optimisation procedure previously used to obtain semi-empirical parameters for the main group elements. The modifications to this procedure for obtaining parameters for transition metal atoms are outlined. In addition to modifications to the semi-empirical core repulsion function, which yield significant improvements in the calculation of molecular structures, compared to the standard core repulsion function, are outlined. The reported parameters are then tested on a set of model complexes containing a variety of ligands and show good agreement with both DFT and experimental data for these species.


*Keywords:* Rubredoxins; PM3; Transition metals; BFGS; Parameterization

## 1. Introduction

Structures in which iron atoms are surrounded by a coordination sphere having a variable number of sulfur atoms are common to many proteins involved in electron-transfer reactions [1]. Rubredoxins (Rd) have a single iron atom surrounded by four cysteine thiolate groups, whilst other proteins have a core with up to four iron atoms [2,3]. The electronic structures of these cores have attracted on-going experimental and theoretical studies, with particular interest in the search for small complexes which display some of the properties of the metal core found in the protein. From a theoretical point of view, these complexes can be valuable in validating computational approaches, which can then be applied to the actual protein [4]. The problems of modelling enzyme structure and reactivity arising from the size of the enzyme, the need to consider molecular motion as well as solvation, are compounded in metalloenzymes, where there is the additional problem of properly describing the metal centre, which can often include the consideration of a range of possible spin states [5].

Density-functional theory (DFT) methods are a popular way of modelling quite large clusters which might be representative of the whole enzyme, but here, apart from the computational expense of including a sufficiently large cluster and its associated motion, there is the ever-present problem of choosing the most appropriate functional [6]. The problem of the size of the enzyme is often tackled by the use of hybrid or embedding methods [7–10], but here again the reactive region of the enzyme is usually treated at a DFT level. The philosophy of using a quantum mechanical method with some adjustable parameters, inherent in a DFT treatment, is, of course, taken much further in semi-empirical methods [11–16]. These methods are now experiencing a renaissance [17] arising from the recognition that it may not be feasible to use DFT methods to treat all of the different aspects of protein structure and reactivity.

For molecular systems without transition metal atoms, it has been recognised that the parameters within the semi-empirical method, appropriate for a particular atom will probably depend upon the bonding environment of that

* Corresponding author. Tel.: +44 161 275 4686; fax: +44 161 275 4734.
*E-mail address:* j.p.mcnamara@manchester.ac.uk (J.P. McNamara).

1093-3263/$ – see front matter © 2005 Elsevier Inc. All rights reserved.
doi:10.1016/j.jmgm.2005.07.001

atom, just as the corresponding parameters in an atomistic force field are bond-dependent. This has been recognised in the specific reaction parameter (SRP) strategy of Truhlar and co-workers, which has been applied to a number of enzyme reactions [18]. We have previously followed this approach in developing parameters within the PM3 scheme to model carbohydrates [19]. This approach is likely to be far from straightforward when applied to systems having transition metal atoms due to the generally greater richness of possible electronic states. We have described a strategy of obtaining the one-centre parameters by fitting to experimental atomic excitation and ionization energies, followed by adjusting the remaining parameters to fit the properties of model compounds which are representative of a particular transition metal-containing core [20]. This approach has resulted in a full set of parameters for iron, which are appropriate for describing various oxidation states of iron–sulfur proteins. When tested on a set of analogues involving a variety of ligands, good agreement was found with both DFT and experimental data for these species [21,22]. The use of these parameters within a two-level ONIOM treatment of the protein Rd was found to give accurate predictions of the effect of the enzyme on both Fe–S bond lengths and inner sphere reorganization energies [21].

We here extend our parameterisation strategy described elsewhere to include a larger training set containing a range of small complexes related to Rd, having Fe–X bonds as well as Fe–S bonds (refer to Table 1). The new parameters have been obtained using a gradient-based optimisation algorithm, which has been used historically to obtain parameters for the main group elements only [11,14]. We therefore outline our implementation of this algorithm and the appropriate modifications for the optimisation of transition metal parameters. The extension of the SRP approach to accurately describe iron-containing proteins will most likely require the modification of the semi-empirical core repulsion function to include bond-specific parameters as proposed for the AM1/d parameterisation of molybdenum [23]. We therefore include details of the semi-empirical core repulsion function and detail our modifications for the study of iron–sulfur proteins.

We first investigate the use of our semi-empirical parameters in the prediction of the structures and reorganisation energies for both Fe(II) and Fe(III) high- and low-spin complexes. We also investigate their prediction of subtle changes in redox properties for both the high spin Fe(II) and Fe(III) states of these complexes and obtain values of the reorganization energies ($\lambda_{oxi}$), values central to discussing electron transfer in terms of Marcus theory [24]. In addition, we explore the use of the parameters to predict the structures of a range of small complexes related to iron–sulfur proteins. A range of complexes involving the binding of the [Fe(py$S_4$)] fragment to various small ligands [e.g. CO, $N_2H_2$, $N_2H_4$, $NH_3$, $C_6H_5N$ and $P(CH_3)_3$], have recently been prepared in which there are two Fe–X interactions in addition to the four Fe–S interactions [25]. These latter

Table 1
Experimental, B3LYP/6–31G* and PM3 structures (Å), VDE, ADE and reorganisation energies ($\lambda_{oxi}$) (eV) of complexes in the training set

| Complex(s)[a] | Fe–X | | | | Energies | DFT | PM3 |
|---|---|---|---|---|---|---|---|
| | Reduced | | Oxidised | | | | |
| | DFT | PM3 | DFT | PM3 | | | |
| $[Fe(SCH_3)_4]^{2-/1-}$ | 2.43 | 2.43 | 2.32 | 2.31 | VDE | −1.90 | −1.52 |
| | | | | | ADE | −2.17 | −2.02 |
| | | | | | $\lambda_{oxi}$ | 0.27 | 0.50 |
| $[Fe(NH_3)_4]^{2+/3+}$ | 2.14 | 2.15 | 2.09 | 2.12 | VDE | 17.18 | 16.69 |
| | | | | | ADE | 17.05 | 16.60 |
| | | | | | $\lambda_{oxi}$ | 0.13 | 0.09 |
| $[FeCl_4]^{2-/1-}$ | 2.41 | 2.40 | 2.23 | 2.24 | VDE | −1.33 | −0.64 |
| | | | | | ADE | −1.99 | −1.60 |
| | | | | | $\lambda_{oxi}$ | 0.66 | 0.96 |
| $[FeBr_3]^{1-/0}$ | 2.38 | 2.37 | 2.28 | 2.26 | VDE | 4.35 | 4.27 |
| | | | | | ADE | 4.17 | 3.89 |
| | | | | | $\lambda_{oxi}$ | 0.18 | 0.38 |
| $[Fe(CN)_6]^{4-/3-}$ | 2.01 | 1.97 | 1.99 | 2.00 | VDE | −9.24 | −9.12 |
| | | | | | ADE | −9.36 | −9.30 |
| | | | | | $\lambda_{oxi}$ | 0.12 | 0.18 |
| $[Fe(SCH_3)_3(OCH_3)]^{2-/1-}$[b] | 2.45 (1.93) | 2.45 (1.92) | 2.33 (1.83) | 2.33 (1.84) | VDE | −2.21 | −1.99 |
| | | | | | ADE | −2.53 | −2.45 |
| | | | | | $\lambda_{oxi}$ | 0.32 | 0.46 |
| $[Fe(CO)_5]$[c] | 1.81 (1.80) | 1.81 (1.79) | | | | | |

[a] All complexes are high spin except for $[Fe(CN)_6]^{4-/3-}$ and $[Fe(CO)_5]$ which are low spin.
[b] Fe–O distances (in parenthesis).
[c] Axial Fe–C distances and (in parenthesis) equatorial Fe–C distances.

complexes are also redox-active, which strengthens their case to be studied as redox-active site analogues. In this paper, we not only investigate the use of our iron parameter set to study these complexes, but explore the use of different density-functionals to describe these new molecules having the [Fe(pyS$_4$)] fragment.

## 2. Optimisation strategy

The power of semi-empirical methods does not lie in their theoretical rigor, but in the flexibility of having adjustable parameters that can be optimised to reproduce important chemical properties [11]. Historically, the objective of semi-empirical parameterisations was to accurately predict the molecular structures and heats of formation at a fraction of the cost needed for ab initio methods [12,13]. Whilst current parameterisations still largely focus on main group elements [14], there has been some effort to extend semi-empirical methods to transition metals [20–23,26]. Although the theoretical framework is relatively straightforward, relatively few parameterisations of transition metals have been published, possibly due in part to the fact that transition metal-containing systems usually have closely spaced energy levels, which make such systems more prone to convergence problems. It is therefore difficult to make the optimisation procedure automatic, as in the case of the main group elements [11,14].

The optimisation of semi-empirical parameters, particularly, for transition metals, is challenging given that the parameter space can contain multiple minima. In any optimisation strategy, a necessary condition common to all approaches is that the error function, $S$ (Eq. (1)), be minimised:

$$S = \sum_i w_i (q_i^{\text{calculated}} - q_i^{\text{reference}})^2 \quad (1)$$

where $q_i^{\text{calculated}}$ and $q_i^{\text{reference}}$ are the calculated (semi-empirical) and reference (usually experiment or high level calculation) molecular quantities and $w_i$ is an appropriate weighting factor. The goal in parameter optimisation is to minimise $S$ efficiently and this can be achieved, with varying degrees of success, using either a genetic algorithm (GA) [18,21,22,26–28] or gradient-based methods [11,14].

### 2.1. Genetic algorithms

Genetic algorithms are based upon Darwin's theory of natural selection and use a series of mathematical operations to mimic natural selectivity. Recently, genetic algorithms have been used to successfully obtain semi-empirical parameters for sodium [27], magnesium [28] and technetium [26] using training sets containing a few tens of reference molecules. For sodium and magnesium, the error function contained contributions from heats of formation, geometric properties, dipole moments and ionisation potentials in line with traditional semi-empirical parameterisation strategies [11–14]. However, in the case of technetium, only geometric properties were included in the training set, thus potentially limiting the applicability of these parameters in the prediction of chemical reaction energetics. With this in mind, we have previously developed a PM3 parameter set for iron using a genetic algorithm in which the one-centre parameters $\{U_{ss}, U_{pp}, U_{dd}, G_{ss}, G_{sd}, G_{dd}, H_{sd}\}$ were fitted to the energies of various electronic states of the neutral and ionised atom and the remaining parameters $\{G_{pp}, \beta_s, \beta_p, \beta_d, \zeta_s, \zeta_p, \zeta_d, \alpha, a_1, a_2, b_1, b_2, c_1, c_2\}$ were fitted to the structures and energies obtained from DFT calculations of active site analogues of Rd, namely $[Fe(SCH_3)_4]^{1-}$ and $[Fe(SCH_3)_4]^{2-}$ [21,22]. These parameters when tested on a set of analogues involving a variety of ligands (for example, $FeCl_4^{2-/1-}$ and $FeBr_3^{1-/0}$) gave good agreement between both DFT and experimental data for these species. However, the extension of semi-empirical methods to study other iron-containing enzymes may require a strategy which includes a larger training set to more fully describe the differing iron environments.

### 2.2. Development of a gradient-based optimisation algorithm

Traditionally, parameters for the main group elements have been obtained for NDDO-based methods (MNDO, AM1 and PM3) using gradient-based minimisation methods in which typically, several hundred parameters (for a variety of elements) are optimised simultaneously [11–14]. Stewart first proposed an efficient optimisation algorithm based upon a modified Broyden–Fletcher–Goldfarb–Shanno (BFGS) method [11]. Details of the BFGS algorithm used herein are described elsewhere [29,30]. A central feature of Stewart's procedure is that the reference structure is taken and the parameters adjusted, until the atomic forces for this structure are minimized, rather than performing explicit geometry optimization.

In the iterative optimization of the parameters, the time-consuming step is the evaluation of the gradients of the error function with respect to the parameters. However, for small changes in $n$ parameters ($x$), any reference property $q$ (e.g. a heat of formation for a reference molecule) can be approximated using a truncated Taylor expansion centred around the initial parameter values ($x^0$) (Eq. (2)) [11].

$$q(x_1, x_2, \ldots, x_n) = q(x_1^0, x_2^0, \ldots, x_n^0) + \sum_{i=1}^{n} \left.\frac{\partial q}{\partial x_i}\right|_{x_i = x_i^0} \cdot (x_i - x_i^0) \quad (2)$$

This allows for the efficient evaluation of the error function ($S$, Eq. (1)) and its gradients at small displacements of the initial parameters. In addition, as suggested by Stewart, a quadratic restraining function is used to prevent large

changes in parameter values [11,14]. After a number of cycles, a further explicit function and gradient calculation is needed due to the build-up of errors.

### 2.3. Modifications to the gradient-based optimisation algorithm for transition metals

The modified BFGS algorithm has been used previously to determine parameters for the main group elements [11–14]. Our approach differs from the optimisation of the AM1/d parameters for molybdenum (the only other reported gradient-based optimisation of transition metal parameters) [23], in that our optimisation approach involves no geometry optimisation. In addition, unlike previous metal parameterisations [23,26], we choose to fit to DFT calculations (rather than experimental data) and also explicitly include information on the atomic charges, spin densities and $\langle S^2 \rangle$ in our fitting function. To obtain parameters for transition metals requires some simple yet important changes to the optimisation algorithm [11,14]. Properties of transition metals are particularly challenging to calculate given their closely lying electronic states which can lead to SCF convergence problems. For this reason, we have developed an efficient DIIS algorithm (which in most calculations can halve the number of SCF iterations required) and a level-shifting algorithm to obtain convergence, within our local semi-empirical code [20]. For explicit calculation of the error function and gradients, the molecular orbitals are stored at each explicit function evaluation ($n$) and these data are read as an initial guess for the ($n + 1$) explicit function evaluation. This has a two-fold effect, firstly it significantly increases the efficiency of the calculations and secondly, it ensures that as the parameters change the error function changes smoothly. This modification prevents significant fluctuations and instability in the error function as the parameters are adjusted.

### 2.4. Choice of the core repulsion function

Semi-empirical methods have greater flexibility to describe a range of different molecules if there is added freedom in the core–core repulsion functions. Within the NDDO approximation, the core–electron attractions ($V_{\mu\nu,\mathrm{B}}$) and core–core repulsions ($E_{\mathrm{AB}}^{\mathrm{MNDO}}$) are expressed in terms of two-centre two-electron integrals (Eqs. (3) and (4)) [31,32]. The form of the core–electron attraction function (Eq. (3)) is common to all NDDO methods, whilst Eq. (4) denotes the form of the core–repulsion function used within the MNDO method:

$$V_{\mu\nu,\mathrm{B}} = -Z_{\mathrm{B}}(\mu^{\mathrm{A}}\nu^{\mathrm{A}}, s^{\mathrm{B}}s^{\mathrm{B}}) \tag{3}$$

$$E_{\mathrm{AB}}^{\mathrm{MNDO}} = Z_{\mathrm{A}}Z_{\mathrm{B}}(s^{\mathrm{A}}s^{\mathrm{A}}, s^{\mathrm{B}}s^{\mathrm{B}})(1 + e^{-\alpha_{\mathrm{A}}R_{\mathrm{AB}}} + e^{-\alpha_{\mathrm{B}}R_{\mathrm{AB}}}) \tag{4}$$

where $Z_{\mathrm{A}}$ and $Z_{\mathrm{B}}$ correspond to the core charges, $R_{\mathrm{AB}}$ the internuclear separation, whilst $\alpha_{\mathrm{A}}$ and $\alpha_{\mathrm{B}}$ are adjustable parameters, where the effect of the core is described by a valence shell ss charge distribution. In MNDO, AM1 and PM3, the two-centre two-electron integral part of the core repulsion function is expressed as (Eqs. (5) and (6)) [11,31,33,34];

$$(s^{\mathrm{A}}s^{\mathrm{A}}, s^{\mathrm{B}}s^{\mathrm{B}}) = \frac{e^2}{(R_{\mathrm{AB}}^2 + (\rho_{\mathrm{A}} + \rho_{\mathrm{B}})^2)^{1/2}} \tag{5}$$

where

$$\rho = \frac{1}{2G_{\mathrm{ss}}} \tag{6}$$

where $R_{\mathrm{AB}}$ is the distance between the centres, $e$ the electronic charge and $G_{\mathrm{ss}}$ is the semi-empirical one-centre, two-electron repulsion integral. The form of the core repulsion function in AM1 and PM3 differs from that used in MNDO in that correlation is accounted for by the inclusion of one to four sets of Gaussian functions (denoted by $a$–$c$, Eq. (7)) [11,33,34].

$$E_{\mathrm{AB}}^{\mathrm{AM1,PM3}} = E_{\mathrm{AB}}^{\mathrm{MNDO}} + \frac{Z_{\mathrm{A}}Z_{\mathrm{B}}}{R_{\mathrm{AB}}}\sum_{i=1}^{4} \times \left[a_{i\mathrm{A}}e^{-b_{i\mathrm{A}}(R_{\mathrm{AB}}-c_{i\mathrm{A}})^2} + a_{i\mathrm{B}}e^{-b_{i\mathrm{B}}(R_{\mathrm{AB}}-c_{i\mathrm{B}})^2}\right] \tag{7}$$

However, for methods which include d orbitals, MNDO/d and AM1/d, it has been found that to obtain the correct balance between attractive and repulsive coulomb interactions requires that $\rho$ (Eq. (6)) is treated as a separate adjustable parameter, which is now used in the evaluation of the interactions given by Eqs. (3) and (4) [15,16]. In their AM1/d parameterisation of molybdenum, Voityuk and Rösch found that using the NDDO core repulsion term (Eq. (4)) led to systematic deviations for some Mo–X bond lengths and the inclusion of additional Gaussian functions did not lead to significantly improved results [23]. This led to a further modification of the core repulsion function in which bond-specific parameters $\alpha_{\mathrm{Mo–X}}$ and $\delta_{\mathrm{Mo–X}}$ were introduced (Eq. (8)) [35]. The idea of using bond-specific core repulsion parameters is not a new one. In the AM1 parameterisation of boron, bond-specific Gaussian-type functions were included in order to improve the final results [36]:

$$E_{\mathrm{Mo–X}}^{\mathrm{AM1/d}} = Z_{\mathrm{Mo}}Z_{\mathrm{X}}(s^{\mathrm{A}}s^{\mathrm{A}}, s^{\mathrm{B}}s^{\mathrm{B}})[1 + 2\delta_{\mathrm{Mo–X}}e^{-\alpha_{\mathrm{Mo–X}}R_{\mathrm{Mo–X}}}] \tag{8}$$

The AM1/d modification of the core repulsion function was found to be much more efficient than introducing Gaussian functions, significantly improving results and has since been used in the extension of MNDO, AM1 and PM3 to the other main group elements [14]. We note that in the case of atom X being hydrogen, the parameter $\delta_{\mathrm{Mo–X}}$ is replaced by the interatomic distance between these atoms (in Å) [23]. This is the form of the core repulsion function adopted in our PM3 parameterisation. Therefore, for iron, the PM3 Gaussian parameters $a$–$c$ are set to zero and there is an additional

adjustable parameter $\rho$, and for each Fe–X interaction separate $\delta_{Fe-X}$ and $\alpha_{Fe-X}$ parameters.

## 3. Computational results

### 3.1. Parameterisation algorithm

Rd has a single iron atom surrounded by four thiolate groups [37]. The electronic structures of this core and related analogues have been the subject of both experimental and theoretical studies, usually involving small complexes, which display some of the properties of the metal core found in the protein [4,38]. For this reason, we chose a training set containing a range of high and low spin iron complexes related to Rd for which experimental and DFT data are available [39–41]. In view of the importance of iron hydrogenases [42], we have also included complexes in which iron is coordinated both $CN^-$ and CO within our training set (refer to Table 1). The final training set contains 13 complexes, which although small, is comparable to the size of training sets used to parameterise some of the main group elements [14]. Given that our strategy is to derive a set of parameters for iron–sulfur proteins, 13 complexes may be sufficient to describe the range of different protein environments.

We have previously shown that the B3LYP [43–45] functional with a 6–31G* basis set can accurately describe various oxidation states of iron–sulfur proteins [21]. In addition, calculations on $[Fe(SCH_3)_4]^{1-}$ using DFT gives a structure in good agreement with the available experimental data [39]. Furthermore, calculation of the adiabatic and vertical detachment energies (ADE, VDE) and reorganisation energies ($\lambda_{oxi}$) for a range of Rd analogues at this level yields energies in close agreement with the experimental data [21]. This gives us confidence that this level of calculation will also give a good description of those species for which no data exist. We note that the DFT calculations reported herein were carried out with the GAUSSIAN 03 suite of programs [46], using either the B3LYP or BP86 [47,48] functional and a 6–31G* basis set.

The error function (Eq. (1)) contained weighted contributions from the internal coordinates of each molecule (as generated by the GAUSSIAN 03 program), charges and spin densities of all atoms, $\langle S^2 \rangle$ of the wavefunction and the relative energies of the redox couples (Table 2). We find that by fitting both charges, spin densities and $\langle S^2 \rangle$ directs the algorithm towards the desired orbital occupations for iron.

Table 2
Weighting factors used in error function

| Property[b] | Scaling factor |
|---|---|
| Fe–X distance gradient[a] (mol Å$^{-1}$ kcal$^{-1}$) | 70 |
| Relative energies (kcal$^{-1}$ mol) | 1000 |
| Spin densities (dimensionless) | 1000 |
| Atomic charges ($e^{-1}$) | 2000 |

[a] Remaining internal coordinate gradients scaled by 0.7 mol Å$^{-1}$ kcal$^{-1}$ [11].
[b] Inverse units used since error function is dimensionless.

The starting parameters were taken as follows: the one-centre terms ($U_{ss}$, $U_{pp}$, $U_{dd}$, $G_{ss}$, $G_{sd}$, $G_{dd}$, $H_{sd}$) were derived using a GA to fit to the electronic states of the neutral and charged atom [20] and the other one-centre ($G_{pp}$) and two-centre terms ($\beta_s$, $\beta_p$, $\beta_d$, $\zeta_s$, $\zeta_p$, $\zeta_d$) were chosen to be those we have previously reported for iron–sulfur proteins [21]. The remaining core–core parameters were assigned values of 1.5 ($\delta_{Fe-X}$) and 2.0 ($\alpha_{Fe-X}$). In order to gain an initial estimate for the values of $\rho$ and $\delta_{Fe-X}$, we first used a small training set containing only the active site analogues of Rd, $[Fe(S-CH_3)_4]^{2-}$ and $[Fe(SCH_3)_4]^{1-}$. These parameters were then used as the initial values in the full optimisation of the larger training set. This approach differs from our previous parameterisation strategy [20–22], in that we allow all the one-centre parameters to be adjusted, since by constraining these parameters led to unrealistic high populations of the 4p valence orbitals of the metal. A similar problem was encountered in the parameterisation of molybdenum [23]. During the optimisation, constraints were imposed upon the allowed values of the parameters, in order to prevent individual parameters changing to unrealistic values, which may limit the transferability of the parameter set to other systems.

In contrast to the GA approach, we were unable to locate a set of parameters to describe $[Fe(SCH_3)_4]^{2-/1-}$ when the training set contained only these two complexes. It is likely that in such gradient-based optimisations a sufficiently large training set must be surveyed in order to identify "false" local minima [11]. In addition, due to the fact that the procedure avoids explicit geometry optimisation, there is the possibility of obtaining parameters which yield very small gradients for the reference structures, but upon geometry optimisation, predict structures that are quite different from the reference ones. By surveying a larger number of reference structures and coordination environments, this effect is somewhat reduced. We also note that the inclusion of B3LYP data for the $[Fe(H_2O)_6]^{3+/2+}$ redox couple led to a significant reduction in the accuracy of the final parameter set. It was decided to omit the hexaaqua complex from our training set in view of the tendency for PM3 to predict relatively short hydrogen–hydrogen interactions of 1.8 Å [49].

In the proposed core repulsion function (Eq. (8)), Voityuk and Rösch suggest that for Mo, the parameter $\delta_{Mo-H}$ is set equal to the interatomic distance, $R_{Mo-H}$ (in Å) [23]. However, for our training set, we found improvements in the final results by allowing $\delta_{Fe-H}$ to be included as an adjustable parameter within the optimisation. The use of the standard PM3 core repulsion function (Eq. (7)), without the bond-specific modifications (Eq. (8)) led to some problems. In particular, there was a tendency for iron to form strong interactions with both carbon and hydrogen atoms in preference to the desired iron–ligand interactions. This may be due in part to the well-documented problems associated

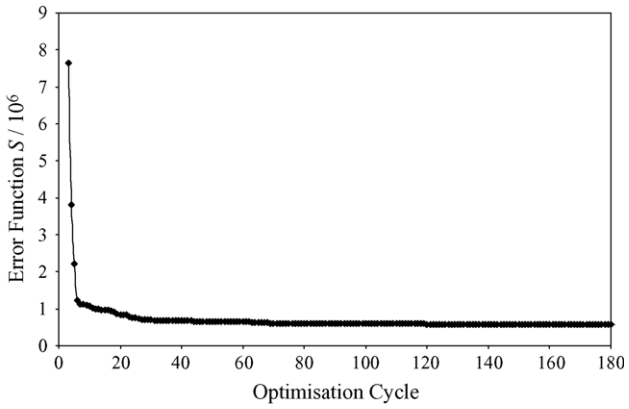


Fig. 1. Minimisation (first 180 cycles) of error function $S$ for the 13 complexes given in Table 1. Data for cycles 1 and 2 omitted for clarity (where $S \sim 9.4 \times 10^7$ and $11.3 \times 10^7$, respectively).

with the PM3 core repulsion function [49]. In particular, it was found that if the ligands contained hydrogen, the coordination at the metal centre could be distorted due to unrealistic hydrogen–hydrogen attractions between ligands [49].

The optimisation of a total of 29 parameters (including 14 bond-specific terms) and a reference training set of 13 complexes, of which the largest molecule contained 21 atoms, took approximately 10 h on a single AMD Opteron CPU. The optimisation involved 553 cycles and 13 explicit function and gradient evaluations, each of which typically involved some 767 SCF and force calculations. In line with Stewart's algorithm [11], we also find that during the initial stages of the optimisation the value of the error function dropped rapidly, partly due to the crude initial guess of the core repulsion parameters ($\rho$, $\delta_{Fe-X}$ and $\alpha_{Fe-X}$). After the first few optimisation cycles, the error function $S$ dropped from $10^8$ to approximately $10^5$ (Fig. 1). The final optimised parameters are given in Table 3.

Table 3
Optimised PM3 parameters for iron

| Parameter[a] | |
|---|---|
| $U_{ss}$ (eV) | −72.975271 |
| $U_{pp}$ (eV) | −51.916356 |
| $U_{dd}$ (eV) | −113.635435 |
| $G_{ss}$ (eV) | 8.280843 |
| $G_{pp}$ (eV) | 7.000075 |
| $G_{dd}$ (eV) | 17.403395 |
| $G_{sd}$ (eV) | 10.853969 |
| $H_{sd}$ (eV) | 0.784914 |
| $\beta_s$ (eV) | −10.473307 |
| $\beta_p$ (eV) | −4.544385 |
| $\beta_d$ (eV) | −22.844986 |
| $\xi_s$ (au) | 1.535819 |
| $\xi_p$ (au) | 1.385013 |
| $\xi_d$ (au) | 2.190100 |
| $\rho$ (au) | 1.373072 |
| $\delta_{Fe-H}$ (dimensionless) | 1.740451 |
| $\delta_{Fe-C}$ (dimensionless) | 0.799631 |
| $\delta_{Fe-N}$ (dimensionless) | 0.744225 |
| $\delta_{Fe-O}$ (dimensionless) | 1.708643 |
| $\delta_{Fe-S}$ (dimensionless) | 1.181990 |
| $\delta_{Fe-Cl}$ (dimensionless) | 1.174521 |
| $\delta_{Fe-Br}$ (dimensionless) | 2.092671 |
| $\alpha_{Fe-H}$ (Å$^{-1}$) | 2.341084 |
| $\alpha_{Fe-C}$ (Å$^{-1}$) | 2.092210 |
| $\alpha_{Fe-N}$ (Å$^{-1}$) | 2.111003 |
| $\alpha_{Fe-O}$ (Å$^{-1}$) | 2.925931 |
| $\alpha_{Fe-S}$ (Å$^{-1}$) | 2.315527 |
| $\alpha_{Fe-Cl}$ (Å$^{-1}$) | 2.342496 |
| $\alpha_{Fe-Br}$ (Å$^{-1}$) | 2.704154 |

[a] Units in parenthesis.

### 3.2. Calculation of complexes in the training set

We first describe the use of our new parameters to predict the structures and properties of the high- and low-spin complexes within the reference DFT data set (Tables 1 and 4). For the high-spin complexes (Table 1), PM3 predicts bond lengths very close to those calculated at the DFT level, the largest discrepancy being for the $[Fe(NH_3)_4]^{3+}$ complex which has Fe–N bonds some 0.03 Å longer than the corresponding DFT values. For all high-spin complexes, PM3 predicts a decrease in the iron ligand distance upon removal of a single electron in line with the DFT calculations. However, for the low spin $[Fe(CN)_6]^{4-}$ complex PM3 predicts an unexpected increase in the Fe–C distances upon ionisation. As far as the ADEs and VDEs are concerned, PM3 yields ADEs which are comparable to those calculated using DFT, the largest difference being for ionisation of $[Fe(NH_3)_4]^{2+}$ which is 0.45 eV larger than the corresponding DFT value, whilst for the $[Fe(OCH_3)(SCH_3)_3]^{2-}$ complex the predicted ADE (−2.45 eV) is very close to the DFT value (−2.53 eV). The calculated VDEs are also in excellent agreement with the

Table 4
PM3 and B3LYP/6–31G* atomic charges (e), spin densities and $\langle S^2 \rangle$ (oxidised state in parenthesis) of complexes in the training set

| Complex(s) | Fe charge | | Fe spin density | | $\langle S^2 \rangle$ | |
|---|---|---|---|---|---|---|
| | DFT | PM3 | DFT | PM3 | DFT | PM3 |
| $[Fe(SCH_3)_4]^{2-/1-}$ | 0.67 (0.66) | 1.38 (1.49) | 3.79 (4.04) | 3.55 (3.55) | 6.00 (8.75) | 6.01 (8.76) |
| $[Fe(NH_3)_4]^{2+/3+}$ | 1.15 (1.45) | 0.49 (0.56) | 3.90 (4.41) | 3.48 (3.58) | 6.00 (8.75) | 6.01 (8.75) |
| $[FeCl_4]^{2-/1-}$ | 0.83 (0.89) | 1.36 (1.41) | 3.85 (4.16) | 3.65 (3.76) | 6.00 (8.75) | 6.01 (8.75) |
| $[FeBr_3]^{1-/0}$ | 0.54 (0.86) | 1.00 (1.00) | 3.71 (4.13) | 3.67 (3.85) | 6.01 (8.75) | 6.01 (8.75) |
| $[Fe(CN)_6]^{4-/3-}$ | 0.01 (0.25) | 1.46 (1.53) | 0.00 (1.09) | 0.00 (1.13) | 0.00 (0.75) | 0.00 (0.77) |
| $[Fe(SCH_3)_3(OCH_3)]^{2-/1-}$ | 0.75 (0.82) | 1.16 (1.23) | 3.79 (4.04) | 3.52 (3.58) | 6.01 (8.76) | 6.01 (8.76) |
| $[Fe(CO)_5]$ | 0.42 | 0.98 | 0.00 | 0.00 | 0.00 | 0.00 |

DFT values, despite the ADEs and not the VDEs being included in the fitting function. The reorganisation energies predicted by PM3 are also in acceptable agreement with the DFT values, but for both high- and low-spin complexes are somewhat larger than the corresponding DFT values. Importantly, the PM3 calculations predict essentially the correct trend in reorganisation energies, with $[FeCl_4]^{2-}$ having a larger value than for $[Fe(SCH_3)_4]^{2-}$, although for the $[Fe(CN)_6]^{4-}$ and $[Fe(NH_3)]^{2+}$ species, the ordering is reversed. Finally, we note that the new PM3 parameters also predict spin densities for iron and $\langle S^2 \rangle$ values comparable to those calculated by DFT, the charges on iron being positive, but somewhat larger in general than the DFT values (Table 4).

We turn now to compare our new iron parameters with those obtained previously using a genetic algorithm [21,22]. It is clear that the modification of the core repulsion function leads to a significant improvement in the description of the some complexes. For example, calculation of $[FeBr_3]^{1-/0}$ using the GA parameters predicts Fe–Br distances of 2.55 and 2.46 Å for the Fe(II) and Fe(III) forms, respectively, which differ somewhat from those calculated at the DFT level (2.38 and 2.28 Å). However, using the parameters obtained herein leads to much improved prediction of the Fe–Br distances (2.37 and 2.26 Å). Whilst it is clear this is not a comparison of the GA/gradient-based methods, it is unlikely that the subtle effects for a whole range of iron protein environments can be described using the standard PM3 core repulsion function alone [11].

Table 5
Experimental, B3LYP/6–31G* and PM3 average Fe–X distances (Å) of test complexes not in the training set

| Complex[a] | CSD reference code[b] | Experiment | DFT | PM3 |
|---|---|---|---|---|
| $[FeCl_3]$ | | | 2.14 | 2.16 |
| $[FeBr_4]^{1-}$ | | | 2.36 | 2.32 |
| $[Fe(SCH_3)_3]$ | | | 2.21 | 2.21 |
| $[Fe(Im)_4]^{3+}$ | | | 2.00[c] | 2.06 |
| $[Fe(SCH_3)_4]^{1-}$ | | | 2.23[d] | 2.26 |
| $[Fe(SC_2H_5)_4]^{1-}$ | CANDAW | 2.27 | | 2.31 |
| $[Fe(S_2\text{-}o\text{-}xyl)_2]^{1-}$ | EBEBUI | 2.27 | | 2.31 |
| $[Fe(Cp)_2]^{1+}$ | BADXUA | 2.04 | | 2.17 |
| $[Fe(S_2C_2N_2S)_2]^{1-}$ | VAGJIX | 2.31 | | 2.27 |
| $[Fe(S_2CS)_3]^{3-}$ | TOSRAU01 | 2.29 | | 2.30 |

[a] All complexes are high spin except for $[Fe(SCH_3)_4]^{1-}$ and $[Fe(Cp)_2]^{1+}$.
[b] Cambridge structural database [41].
[c] Ref. [40].
[d] Ref. [50].

### 3.3. Calculation of complexes not in the training set

We first investigate the use of the new parameters for the prediction of the structures of a range of small complexes related to iron–sulfur proteins, which are not part of the training set (refer to Table 5). Evidently the new parameters predict structures comparable with both DFT and the available experimental data [41]. The predicted Fe–N distance (2.06 Å) in the $[Fe(Im)_4]^{3+}$ complex is quite close to the DFT value of 2.00 Å. The largest difference between PM3 and experiment is for ferrocene, for which the PM3 method predicts a Fe–C distance some 0.13 Å longer than

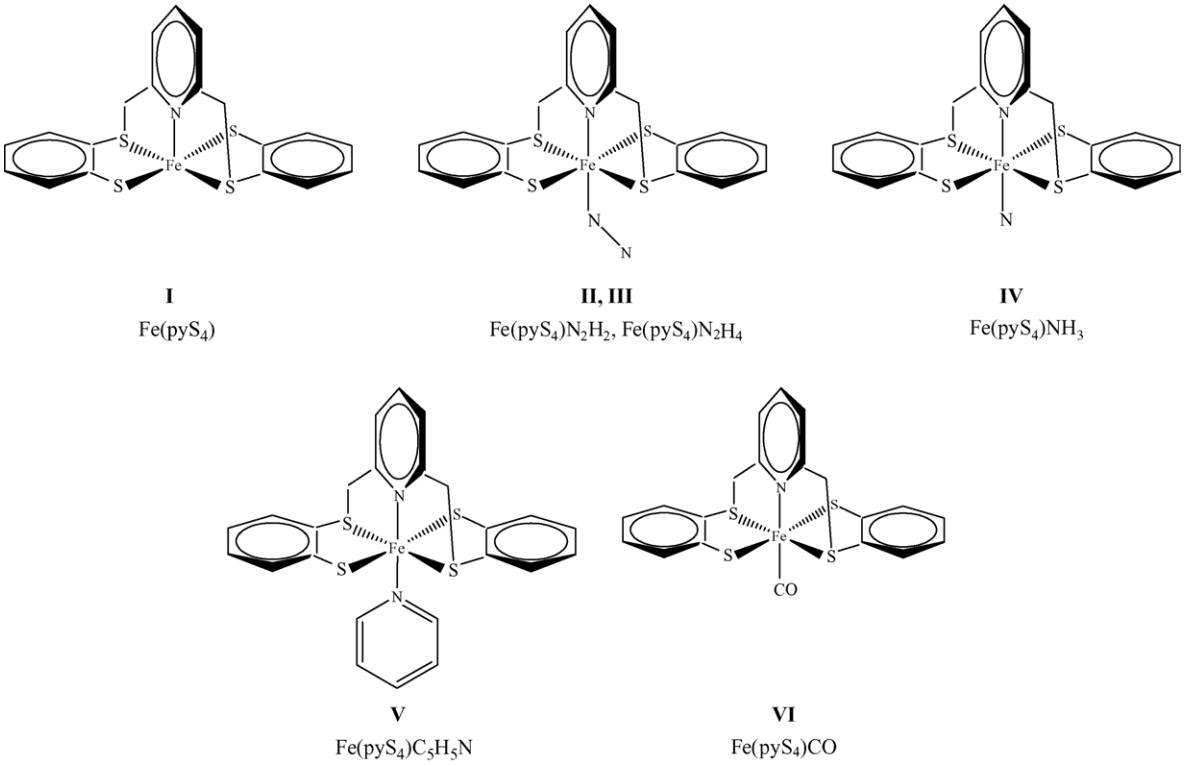


Fig. 2. Test complexes containing the $Fe(pyS_4)$ core (Table 6). Hydrogens are omitted for clarity.

experiment. However, given that the training set is relatively small compared to those used for the main group elements [14], the results are particularly encouraging.

The $[Fe(Im)_4]^{2+/3+}$ complex (Table 5) was not part of the training set, but the new parameters predict on oxidation a change in Fe–N bond length (0.09 Å) and a reorganisation energy (0.38 eV) close to the DFT values (0.08 Å and 0.24 eV), thus giving us confidence to use these parameters to predict the structures of other complexes in which iron is bound to nitrogen-containing ligands. We turn now to a consideration of the model compounds I–VI, involving the $Fe(pyS_4)$ core (see Fig. 2) [25]. In Table 6, we show a comparison of the experimental Fe–X bond lengths with the values predicted by the two different density-functionals and by PM3. As far as the Fe–S bond lengths are concerned, when judged by standard deviations the BP86 functional (0.0258) is superior to B3LYP (0.0645) when compared to experiment. For all the complexes, the PM3-calculated Fe–S distances are generally quite close to the DFT values, whilst the $Fe–N_{pyr}$ distances vary considerably depending on the nature of the second axial ligand. When the second axial ligand is $N_2H_2$ or CO, the iron–ligand bond length is quite well predicted by PM3, but the agreement with experiment is somewhat inferior to the DFT values. Surprisingly, when the ligand is $NH_3$, the $Fe–NH_3$ distance is quite poorly predicted, being some 0.14 Å longer than the B3LYP value. This is probably due in part to limitations in the training set, which only contains essentially one complex where iron is bound directly to nitrogen.

Table 6
Experimental, B3LYP, BP86 and PM3 Fe–X distances (Å) for model complexes I–VI containing $Fe(pyS_4)$ core

| Complex[a] | X[b] | Crystal[c] | DFT | | PM3 |
|---|---|---|---|---|---|
| | | | B3LYP | BP86 | |
| **I** | $N_{pyr}$ | 2.01 | 1.90 | 2.01 | 1.68 |
| | $S_1$ | 2.31 | 2.29 | 2.29 | 2.32 |
| | $S_2$ | 2.29 | 2.30 | 2.30 | 2.32 |
| | $S_3$ | 2.23 | 2.27 | 2.23 | 2.26 |
| | $S_4$ | 2.23 | 2.28 | 2.23 | 2.26 |
| **II** | $N_{pyr}$ | 1.96 | 1.97 | 1.89 | 1.73 |
| | $S_1$ | 2.29 | 2.38 | 2.33 | 2.34 |
| | $S_2$ | 2.31 | 2.37 | 2.33 | 2.34 |
| | $S_3$ | 2.21 | 2.29 | 2.22 | 2.33 |
| | $S_4$ | 2.23 | 2.29 | 2.22 | 2.33 |
| | $N_2H_4$ | 2.04 | 2.04 | 2.01 | 2.41 |
| **III** | $N_{pyr}$ | | 2.01 | 1.97 | 2.15 |
| | $S_1$ | | 2.36 | 2.34 | 2.37 |
| | $S_2$ | | 2.37 | 2.36 | 2.38 |
| | $S_3$ | | 2.30 | 2.24 | 2.31 |
| | $S_4$ | | 2.30 | 2.25 | 2.33 |
| | $N_2H_2$ | | 1.85 | 1.85 | 1.81 |
| **IV** | $N_{pyr}$ | | 1.96 | 1.88 | 1.79 |
| | $S_1$ | | 2.37 | 2.34 | 2.36 |
| | $S_2$ | | 2.37 | 2.33 | 2.36 |
| | $S_3$ | | 2.29 | 2.22 | 2.33 |
| | $S_4$ | | 2.29 | 2.22 | 2.33 |
| | $NH_3$ | | 2.05 | 2.04 | 2.19 |
| **V** | $N_{pyr}$ | 1.96 | 1.98 | 1.92 | 2.02 |
| | $S_1$ | 2.31 | 2.38 | 2.35 | 2.36 |
| | $S_2$ | 2.31 | 2.38 | 2.35 | 2.33 |
| | $S_3$ | 2.23 | 2.29 | 2.22 | 2.32 |
| | $S_4$ | 2.23 | 2.29 | 2.22 | 2.31 |
| | $NC_5H_5$ | 2.00 | 2.02 | 1.98 | 2.07 |
| **VI** | $N_{pyr}$ | 2.01 | 2.04 | 2.01 | 2.15 |
| | $S_1$ | 2.31 | 2.36 | 2.34 | 2.37 |
| | $S_2$ | 2.29 | 2.36 | 2.34 | 2.37 |
| | $S_3$ | 2.23 | 2.29 | 2.24 | 2.30 |
| | $S_4$ | 2.23 | 2.29 | 2.24 | 2.30 |
| | CO | 1.76 | 1.77 | 1.73 | 1.75 |

[a] For structures refer to Fig. 2. All complexes are neutral and low spin. $N_{pyr}$ is the nitrogen of the pyridine ring of the $pyS_4$ core.
[b] $S_3$ and $S_4$ are the tri-coordinated sulfurs.
[c] Ref. [25].

## 4. Conclusions

The results of the calculations described herein give encouragement to the strategy of developing PM3 parameters for transition metal atoms in specific enzyme environments. We have described the modifications of the optimisation procedure used to obtain parameters for the main group elements, in order to use this approach to obtain parameters for transition metal systems. Furthermore, our approach has demonstrated that suitable parameters can be obtained by fitting to DFT calculations alone, whilst including data concerning the wavefunction of the training set can help to direct the optimisation algorithm towards the desired electronic states of the metal centre. The results reported herein compare favourably with those reported using parameters obtained using a GA [21,22].

For transition metals, it is clear that the use of a bond-specific core repulsion function provides the flexibility to describe the complex interactions required to describe differing protein environments [23]. However, given that the form of our core repulsion function for iron–hydrogen interactions differs from that reported for molybdenum–hydrogen interactions, further modifications of this function, particularly for hydrogen–hydrogen and metal–hydrogen interactions may provide additional improvements in the accuracy of these methods [49].

Whilst the training set used herein is comparatively small, the parameter set obtained gives structures and energies in good agreement with experiment, particularly for those in which iron was coordinated to sulfur. This could be due in part to a biasing of the initial parameters, some of which were from an already GA optimised set for iron–sulfur proteins [21,22] and the new core repulsion parameters ($\rho$, $\delta_{Fe–X}$ and $\alpha_{Fe–X}$), which were "pre-optimised" for the Rd redox couple $[Fe(SCH_3)_4]^{2-/1-}$. However, increasing the size of the training set is likely to further improve the transferability of the parameters to study a wider range of protein environments.

The success of our parameterisation strategy for iron–sulfur proteins in treating the effect that both different

ligands and the environment have on different oxidation states of the metal centre, justifies further exploration and improvement of this cost-effective approach of modelling complex metalloenzymes.

## Acknowledgments

We thank EPSRC for support of this work and J.J.P. Stewart for helpful discussion.

## References

[1] W. Lovenberg, Iron–Sulfur Proteins, vol. I, Academic Press, New York, 1973.
[2] P.J. Stephens, D.R. Jollie, A. Warshel, Protein control of redox potentials of iron–sulfur proteins, Chem. Rev. 96 (1996) 2491–2513.
[3] R.H. Holm, P. Kennepohl, E.I. Solomon, Structural and functional aspects of metal sites in biology, Chem. Rev. 96 (1996) 2239–2314.
[4] X.-B. Wang, L.-S. Wang, Probing the electronic structure of redox species and direct determination of intrinsic reorganization energies of electron transfer reactions, J. Chem. Phys. 112 (2000) 6959–6962.
[5] R.A. Torres, T. Lovell, L. Noodleman, D.A. Case, Density functional and reduction potential calculations of $Fe_4S_4$ clusters, J. Am. Chem. Soc. 125 (2003) 1923–1936.
[6] C. Morgado, J.P. McNamara, I.H. Hillier, M. Sundararajan, The structure and spin-states of some Fe(III) mimics of nitrile hydratase, studied by DFT and ONIOM (DFT:PM3) calculations, Mol. Phys. 103 (2005) 905–923.
[7] F. Maseras, K. Morokuma, IMOMM: a new integrated ab initio + molecular mechanics geometry optimisation scheme of equilibrium structures and transition states, J. Comput. Chem. 16 (1995) 1170–1179.
[8] T. Vreven, K. Morokuma, O. Farkas, H.B. Schlegel, M.J. Frisch, Geometry optimisation with QM/MM, ONIOM and other combined methods. Part I: microiterations and constraints, J. Comput. Chem. 24 (2003) 760–769.
[9] J. Gao, X. Xia, A priori evaluation of aqueous polarization effects through Monte Carlo QM–MM simulations, Science 258 (1992) 631–635.
[10] M.J. Field, P.A. Basch, M. Karplus, A combined quantum mechanical and molecular potential for molecular dynamics simulations, J. Comput. Chem. 11 (1990) 700–733.
[11] J.J.P. Stewart, Optimisation of parameters for semiempirical methods. Part I: method, J. Comput. Chem. 10 (1989) 209–220.
[12] J.J.P. Stewart, Optimisation of parameters for semiempirical methods. Part II: applications, J. Comput. Chem. 10 (1989) 221–264.
[13] J.J.P. Stewart, Optimisation of parameters for semiempirical methods. Part III: extension of PM3 to Be, Mg, Zn, Ga, Ge, As, Se, Cd, In, Sn, Sb, Te, Hg, Tl, Pb and Bi, J. Comput. Chem. 12 (1991) 320–341.
[14] J.J.P. Stewart, Optimisation of parameters for semiempirical methods. Part IV: extension of MNDO, AM1 and PM3 to more main group elements, J. Mol. Model 10 (2004) 155–164.
[15] W. Thiel, A.A. Voityuk, Extension of the MNDO formalism to d orbitals: integral approximations and preliminary numerical results, Theor. Chim. Acta 81 (1992) 391–404.
[16] W. Thiel, A.A. Voityuk, Erratum. Extension of the MNDO formalism to d orbitals: integral approximations and preliminary numerical results, Theor. Chim. Acta 93 (1996) 315.
[17] T. Clark, Quo Vadis semiempirical MO-theory? J. Mol. Struct. (Theochem.) 530 (2000) 1–10.
[18] I. Rossi, D.G. Truhlar, Parameterization of NDDO wavefunctions using genetic algorithms: an evolutionary approach to parameterizing potential energy surfaces and direct dynamics calculations of organic reactions, Chem. Phys. Lett. 233 (1995) 231–236.
[19] J.P. McNamara, A.-M. Muslim, H. Abdel-Aal, H. Wang, I.H. Hillier, R.A. Bryce, Towards a quantum mechanical force field for carbohydrates: a reparameterized semi-empirical MO approach, Chem. Phys. Lett. 394 (2004) 429–436.
[20] M. Mohr, J.P. McNamara, H. Wang, S.A. Rajeev, J. Ge, C.A. Morgado, I.H. Hillier, The use of methods involving semi-empirical molecular orbital theory to study the structure and reactivity of transition metal complexes, Faraday Discuss. 124 (2003) 413–428.
[21] M. Sundararajan, J.P. McNamara, I.H. Hillier, H. Wang, N.A. Burton, The development of a PM3 parameter set to describe iron–sulfur proteins, Chem. Phys. Lett. 404 (2005) 9–12.
[22] M. Sundararajan, J.P. McNamara, M. Mohr, H. Wang, I.H. Hillier, A semi-empirical molecular orbital scheme to study electron transfer in iron–sulfur proteins, Biochem. Soc. Trans. 33 (2005) 20–21.
[23] A.A. Voityuk, N. Rösch, AM1/d parameters for molybdenum, J. Phys. Chem. A 104 (2000) 4089–4093.
[24] R.A. Marcus, N. Sutin, Electron transfers in chemistry and biology, Biochim. Biophys. Acta 811 (1985) 265–322.
[25] D. Sellmann, K.P. Peters, F.W. Heinemann, New pentadentate carboxylate-derivatized sulfur ligands affording water soluble iron complexes with $[Fe(NS_4)]$ cores that bind small molecules (CO, NO, $PMe_3$) as co-ligands, Eur. J. Inorg. Chem. 3 (2004) 581–590.
[26] T.R. Cundari, J. Deng, W. Fu, PM3(tm) parameterisation using genetic algorithms, Int. J. Quant. Chem. 77 (2000) 421–432.
[27] E.N. Brothers, K.M. Merz Jr., Sodium parameters for AM1 and PM3 optimised using a modified genetic algorithm, J. Phys. Chem. B 106 (2002) 2779–2785.
[28] M.C. Hutter, J.R. Reimers, N.S. Hush, Modelling the bacterial photosynthetic reaction centre. Part 1: magnesium parameters for the semiempirical AM1 method developed using a genetic algorithm, J. Phys. Chem. B 102 (1998) 8080–8090.
[29] R.H. Byrd, P. Lu, J. Nocedal, C. Zhu, A limited memory algorithm for bound constrained optimization, Siam. J. Sci. Comput. 16 (1995) 1190–1208.
[30] C. Zhu, R.H. Byrd, P. Lu, J. Nocedal, L-BFGS-B, A limited memory FORTRAN code for solving bound constrained optimization problems, Technical Report, EECS Department, Northwestern University, 1994.
[31] M.J.S. Dewar, W. Thiel, Ground states of molecules. Part 38: the MNDO method. Approximations and parameters, J. Am. Chem. Soc. 99 (1977) 4899–4907.
[32] J.J.P. Stewart, MOPAC: a semiempirical molecular orbital program, J. Comput. Aided Mol. Des. 4 (1990) 1–105.
[33] M.J.S. Dewar, E.G. Zoebisch, E.F. Healy, J.J.P. Stewart, AM1: A new general purpose quantum mechanical molecular model, J. Am. Chem. Soc. 107 (1985) 3902–3909.
[34] M.J.S. Dewar, E.G. Zoebisch, E.F. Healy, J.J.P. Stewart, Additions and corrections. AM1: a new general purpose quantum mechanical molecular model, J. Am. Chem. Soc. 115 (1993) 5348.
[35] Eq. (8) differs from the one given in reference [23]; in the original publication, the factor of ‘‘2’’ was inadvertently omitted.
[36] M.J.S. Dewar, C. Jie, E.G. Zoebisch, AM1 calculations for compounds containing boron, Organometallics 7 (1988) 513–521.
[37] S. Niu, X.-B. Wang, J.A. Nicolas, L.-S. Wang, T. Ichiye, Combined quantum chemistry and photoelectron spectroscopy study of the electronic structure and reduction potentials of rubredoxin redox site analogues, J. Phys. Chem. A 107 (2003) 2898–2907.
[38] X. Yang, X.-B. Wang, Y.J. Fu, L.-S. Wang, On the electronic structure of [1Fe] Fe–S complexes from anionic photoelectron spectroscopy, J. Phys. Chem. A 107 (2003) 1703–1709.
[39] L.E. Maelia, M. Millar, S.A. Koch, General synthesis of iron(III) tetrathiolate complexes: structural and spectroscopic models for the $[Fe(Cys–S)_4]$ center in oxidized rubredoxin, Inorg. Chem. 31 (1992) 4594–4600.
[40] E. Sigfridsson, M.H.M. Olsson, U. Ryde, Inner-sphere reorganisation energy of iron–sulfur clusters studied with theoretical methods, Inorg. Chem. 40 (2001) 2509–2519.

[41] F.H. Allen, The Cambridge structural database: a quarter of a million crystal structures and rising, Acta Crystallogr. B 58 (2002) 380–388.
[42] F.A. Armstrong, Hydrogenases: active site puzzles and progress, Curr. Opin. Chem. Biol. 8 (2004) 133–140.
[43] A.D. Becke, Density-functional thermochemistry. Part III: the role of exact exchange, J. Chem. Phys. 98 (1993) 5648–5652.
[44] B. Miehlich, A. Savin, H. Stoll, H. Preuss, Results obtained with the correlation energy density functionals of Becke and Lee, Yang and Parr, Chem. Phys. Lett. 157 (1989) 200–206.
[45] C. Lee, W. Yang, R.G. Parr, Development of the Colle–Salvetti correlation-energy formula into a functional of the electron density, Phys. Rev. B 37 (1988) 785–789.
[46] M.J. Frisch, G.W. Trucks, H.B. Schlegel, G.E. Scuseria, M.A. Robb, J.R. Cheeseman, J.A. Montgomery, Jr., T. Vreven, K.N. Kudin, J.C. Burant, J.M. Millam, S.S. Iyengar, J. Tomasi, V. Barone, B. Mennucci, M. Cossi, G. Scalmani, N. Rega, G.A. Petersson, H. Nakatsuji, M. Hada, M. Ehara, K. Toyota, R. Fukuda, J. Hasegawa, M. Ishida, T. Nakajima, Y. Honda, O. Kitao, H. Nakai, M. Klene, X. Li, J.E. Knox, H.P. Hratchian, J.B. Cross, V. Bakken, C. Adamo, J. Jaramillo, R. Gomperts, R.E. Stratmann, O. Yazyev, A.J. Austin, R. Cammi, C. Pomelli, J.W. Ochterski, P.Y. Ayala, K. Morokuma, G.A. Voth, P. Salvador, J.J. Dannenberg, V.G. Zakrzewski, S. Dapprich, A.D. Daniels, M.C. Strain, O. Farkas, D.K. Malick, A.D. Rabuck, K. Raghavachari, J.B. Foresman, J.V. Ortiz, Q. Cui, A.G. Baboul, S. Clifford, J. Cioslowski, B.B. Stefanov, G. Liu, A. Liashenko, P. Piskorz, I. Komaromi, R.L. Martin, D.J. Fox, T. Keith, M.A. Al-Laham, C.Y. Peng, A. Nanayakkara, M. Challacombe, P.M.W. Gill, B. Johnson, W. Chen, M.W. Wong, C. Gonzalez, J.A. Pople, GAUSSIAN 03 (Revision C.02), Gaussian Inc., Wallingford CT, 2004.
[47] A.D. Becke, Density-functional exchange-energy approximation with correct asymptotic behaviour, Phys. Rev. A 38 (1988) 3098–3100.
[48] J.P. Perdew, Density-functional approximation for the correlation energy of the inhomogeneous electron gas, Phys. Rev. B 33 (1986) 8822–8824.
[49] G.I. Csonka, J.G. Ángyán, The origin of the problems with the PM3 core repulsion function, J. Mol. Struct. (Theochem.) 393 (1997) 31–38.
[50] E. Sigfridsson, M.H.M. Olsson, U. Ryde, A comparison of the inner-sphere reorganisation energies of cytochromes, iron–sulfur clusters and blue copper proteins, J. Phys. Chem. B 105 (2001) 5546–5552.